C. R. Geoscience 344 (2012) 149–158

Contents lists available at SciVerse ScienceDirect

Comptes Rendus Geoscience

www.sciencedirect.com

Tectonics, tectonophysics

Tectonic and geoelectric structures of rift basins in the Baikal region

Structures tectoniques et géo-électriques des bassins de rift de la région du Baïkal

Oxana V. Lunina [a,*], Nina N. Nevedrova [b], Andrei S. Gladkov [a]

[a] *Institute of the Earth's Crust SB RAS, Lermontov Street 128, Irkutsk 664033, Russia*
[b] *Institute of Petroleum Geology and Geophysics SB RAS, Academician Koptyug Pr. 3, Novosibirsk 630090, Russia*

ARTICLE INFO

Article history:
Received 15 February 2011
Accepted after revision 19 December 2011
Available online 13 March 2012

Written on invitation of the Editorial Board

Keywords:
Rift basins
Faults
Geoelectric investigations
Baikal region

Mots clés :
Bassins de rift
Failles
Investigations géo-électriques
Région du Baïkal

ABSTRACT

The article summarizes results of tectonophysical and geoelectric studies of rift basins in the Baikal region. Their sedimentary cover is intersected by faults, which induce shallow soft deformations in Late Cenozoic sediments. The faults observed in the internal part of the basins correlate with zones of contrast change in the deep structures of the crystalline basement and sedimentary layers. They offset the top of the basement and bottom of the sedimentary layers, and constitute zones of lower resistivity values. Significant variations of electrical parameters can be due to redistribution of conducting fluids in a geological massif, which allows discriminating water-bearing faults from water-free ones. Taken as a whole, the tectonic structure of the basins is best defined by the presence of shallow deformation zones, an asymmetrical morphology and fault-block pattern of both the sedimentary infill and basement of the basins.

RÉSUMÉ

L'article résume les résultats d'études tectonophysiques et géo-électriques de bassins de rift dans la région du Baïkal. Leur couverture sédimentaire est traversée de failles qui induisent des déformations peu importantes et peu profondes dans les sédiments du Cénozoïque supérieur. Les failles observées dans la partie interne des bassins se corrèlent avec des zones à changements contrastés, dans les structures profondes du soubassement cristallin et des lits sédimentaires. Elles décalent le sommet du soubassement et la base des lits sédimentaires et constituent des zones de moindre résistivité. Des variations significatives des paramètres électriques peuvent être dues à la redistribution des fluides conducteurs dans un massif rocheux qui permet une discrimination entre failles à circulation d'eau et failles sans circulation d'eau. Prise dans son ensemble, la structure tectonique des bassins est mieux définie par la présence de zones de déformations de faible profondeur, une morphologie asymétrique et une compartimentalisation à la fois du remplissage sédimentaire et du soubassement des bassins.

1. Introduction

During several years, two work teams independently carried out research on the inner structure of rift basins in the Baikal region (Fig. 1). The first team generated maps of fault-block structures and state of stresses of the Earth's crust (Lunina and Gladkov, 2004, 2007, 2008). It showed that Pliocene-Quaternary basin deposits sensitively react to tectonic movements of the crystalline basement as evidenced by deformations of soft and poorly consolidated sediments exposed in natural and artificial outcrops. Many previous fault investigations in the Baikal rift zone, and relevant maps, were based mainly on structural

* Corresponding author.
E-mail address: lounina@crust.irk.ru (O.V. Lunina).

1631-0713/$ – see front matter
doi:10.1016/j.crte.2011.12.008

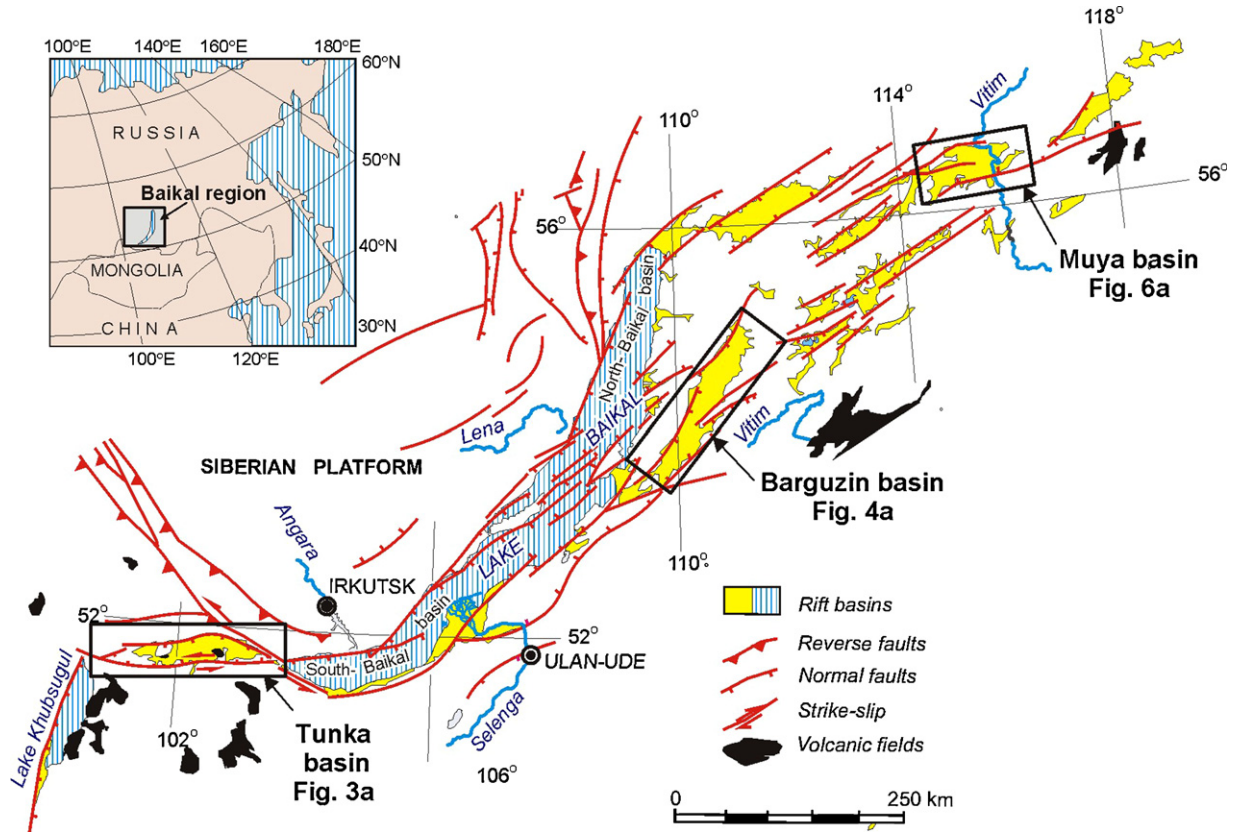

Fig. 1. Simplified structural map of the Baikal region and locations of the rift basins.

Fig. 1. Carte structurale simplifiée de la région du Baïkal et localisation des bassins de rift.

observations of basement rocks as well as on seismic and geomorphologic data (Delvaux et al., 1997; Levi et al., 1982, 1997; Sherman et al., 1973; Solonenko, 1981). Studies of specific sedimentary structures were simultaneously carried out elsewhere in the world (Chunga et al., 2007; Hippolyte, 2001; Obermeier, 1996; Papathanassiou et al., 2005; Sims, 1975; Tuttle et al., 2002).

The second team investigated the geoelectric structure of the rift basins down to basement depths (Epov et al., 2007; Nevedrova and Epov, 2003).

This article aims at presenting the results of integrated data analysis that allow one to obtain a new knowledge about the tectonic structure of the rift basins and to demonstrate the efficiency of applying combined methods to fault mapping in areas covered by Late Cenozoic sediments.

2. Geological background

The basins studied are located between northern Mongolia and southern Yakutia, along a 2200 km long curved band. The basin system, together with adjacent topographic shoulders, make up the Baikal Rift Zone (Fig. 1). Contrasted morphology, Neogene-Quaternary volcanism on flanks of the rift zone, geophysical anomalies and almost ubiquitous thinning of the Earth's crust are general features shared by the Baikal rift with other rift basins. The depressions are superimposed on high-metamorphic structural complexes of Upper Archaean, Proterozoic and Early Paleozoic ages. They are clear indicators of the Cenozoic geodynamic reactivation of the crystalline basement.

According to Logatchev's general conclusion (Logatchev, 2003), the basin subsidence started in the South-Baikal depression near the delta of the Selenga River from the end of Cretaceous to the beginning of Paleocene. Thereafter, a new river system formed, erosion and surface runoff began, resulting in the interconnection of all the former hydrosystems of the western Trans-Baikal region and northern Mongolia, inherited from Late Mesozoic. The basins developed subsequently and some of them appeared only in the Pliocene-Pleistocene epochs. The sedimentary complex in most of the large basins is subdivided into two parts: the lower sedimentary strata consist of Paleocene, Eocene, Oligocene and Miocene deposits, mainly represented by sandstones, siltstones, mudstones and clay with coal layers, as well diatomites and chalky clays; whereas the upper sedimentary strata are dominated by coarse Pliocene-Quaternary debris. The architecture of Cenozoic basins depends on heterogeneities of the crystalline basement at all structural organizational levels, and firstly on Pre-Cenozoic faults. At the same time, this dependence is locally disturbed because of a mismatch among:

- the principal NW-SE direction of tension controlling the basin development;

- the strike of pre-existing faults and other structures of the fold belt, thus implying that rifting obliquely dissected the older basement structures.

There exist two distinct evolutionary models for the region during the Cenozoic. The first one explains the formation of the Baikal rift zone as a result of the Indo-Eurasian collision (Molnar and Tapponnier, 1975) due to transformation of compressional stresses at the plate boundary into tensional stresses at the southern margin of the Siberian craton. According to the second model, the Baikal rift zone developed in two stages of successively slow, and quick riftings caused by the rise of an astenospheric dom, which induced a progressive isostatic uplift (Logatchev and Zorin, 1987). The discussion about the passive versus active riftings is still continuing today.

3. Methodology

Mapping and study of basement-involving fault-block structures, topographic depressions and adjacent rift shoulders were carried out, applying a unified methodological approach that included morphotectonic analysis of the topographical relief, field structural and tectonophysical investigations, as well as examination of available maps more particularly regarding fault tectonics (Lunina and Gladkov, 2004, 2007, 2008). When investigating active faults, the characteristic of both brittle and plastic deformations of the Late Cenozoic deposits (Fig. 2) played a key role. Therefore, observation sites were selected both in bedrocks, as well as in soft and poorly consolidated sediments (Figs. 3, 4, 6, discussed later).

The geoelectric investigations were carried out based on the field data acquired in the middle of the last century through the vertical electrical sounding (VES) method using source lines up to 10 to 16 km long. The average offset between VES points was 2 km long. These surveys aimed at studying the sedimentary infill of the main depocenters, the thickness of which reaching 2 to 3 km. The data collected at that time had initially been processed with a limited scope; therefore we applied up-to-date interpretation tools, which allowed new qualitative results to be inferred.

Processing the experimental geoelectric data was performed by applying automated modeling programs and inversion systems. Geoelectric models were first constructed by using the SONET (Epov et al., 1990) and IPI (Khmelevsky and Shevnina, 1992) software systems. A layer model was considered at each measurement point to be homogeneous. The two-dimensional architecture of geological sections was constructed from individual homogenous blocks of arbitrary geometry using the IE2DP1 program (Khmelevsky and Shevnina, 1992). The forward problem was solved by the integral equation method. Tracing the distribution of lateral heterogeneities

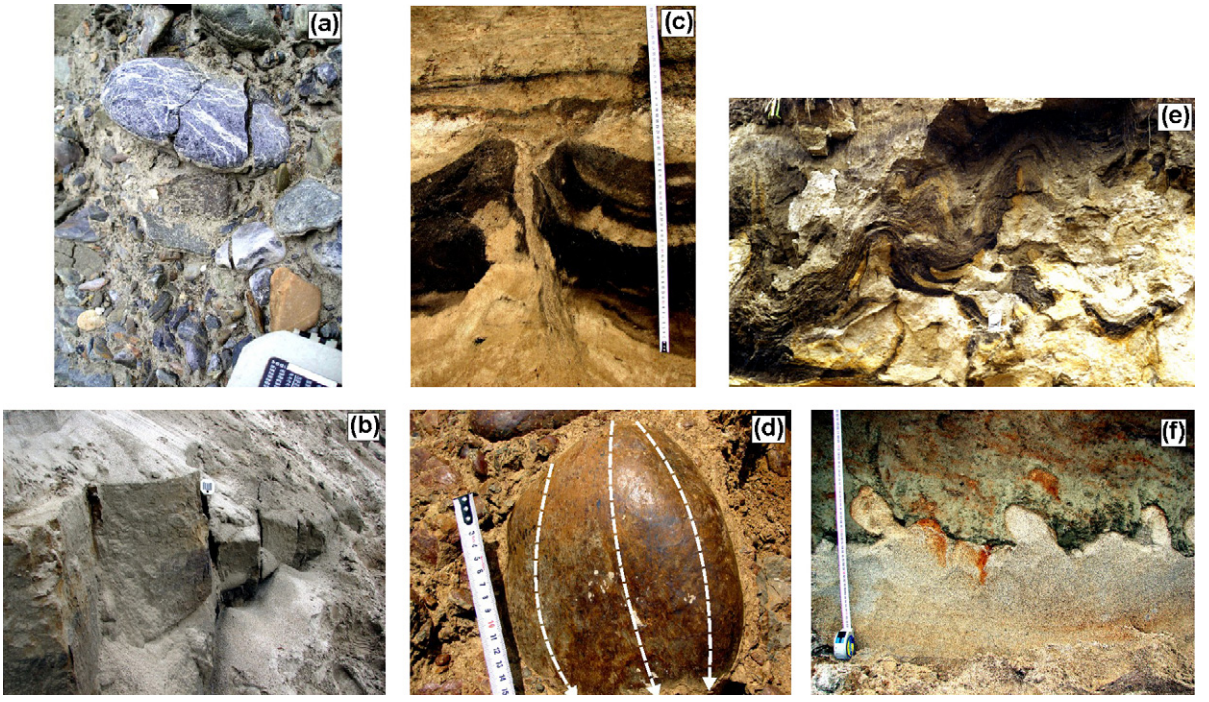

Fig. 2. Examples of Pliocene-Quaternary deformations of soft and poorly consolidated sediments formed under brittle (a–b), brittle-plastic (c–d) and plastic (e–f) conditions in the rift basins of the Baikal region: a: fractures in boulder-pebble sediments; b: fracturing zone in loams; c: injective sandy dike breaking through paleosoil layer; d: slickensides on pebble surface; e: folds of paleosoils in loams and sands; f: seismites (sands are below, loams – above).

Fig. 2. Exemples de déformations plio-quaternaires de sédiments meubles et mal consolidés, formées dans des conditions cassantes (a–b), plastiques-cassantes (c–d) et plastiques (e–f) dans les bassins de rift du Baïkal : a : fractures dans des sédiments à blocs et galets ; b : zone de fracturation dans des matériaux limoneux ; c : dyke d'injection sableux cassant à travers un horizon de paléosol ; d : *slickensides* à la surface d'un galet ; e : plis de paléosols dans des matériaux limoneux ; f : séismites (les sables sont en dessous et les limons au-dessus).

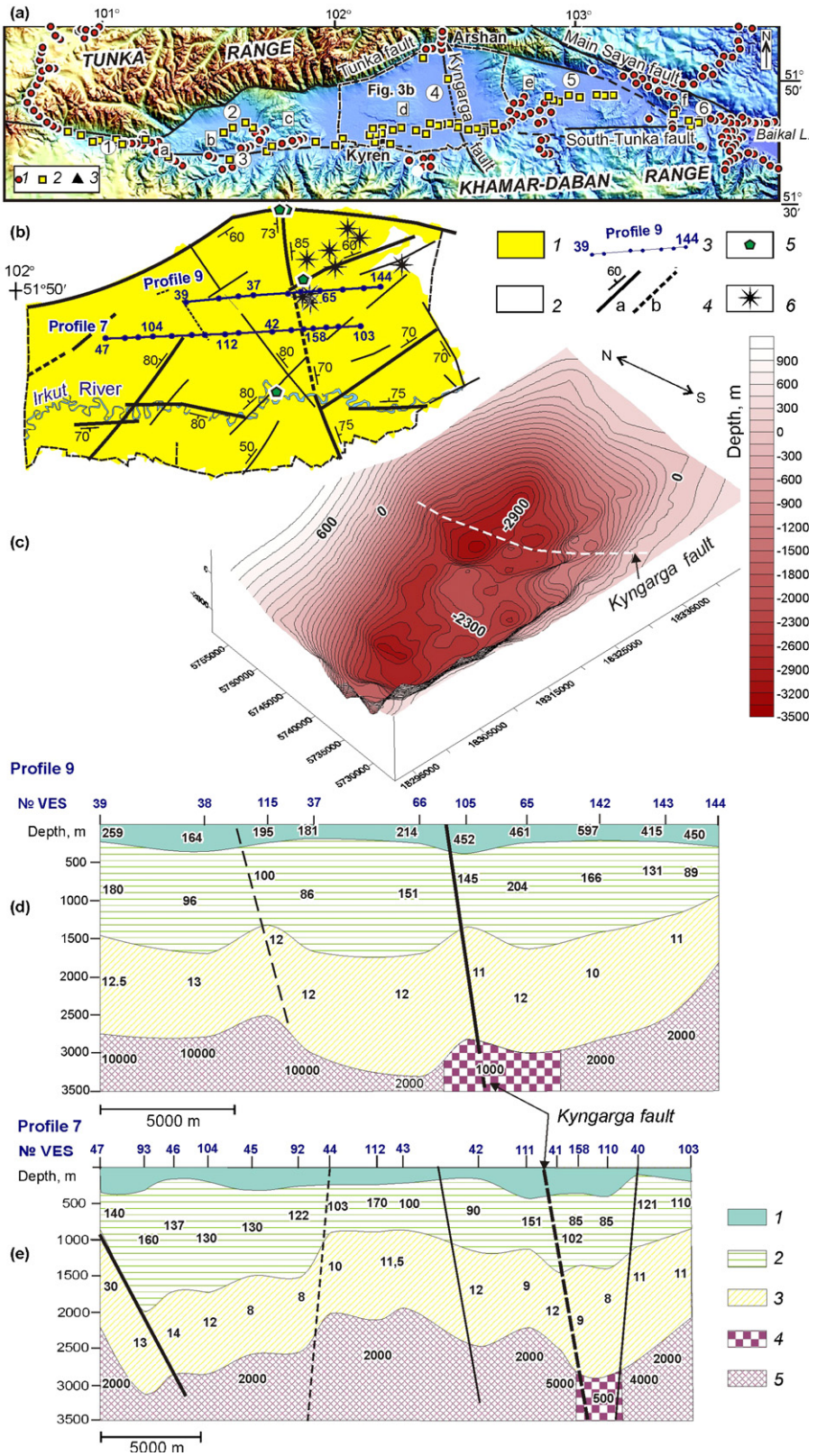

Fig. 3. The Tunka rift basin; Fig. 1 for location: **a**: regional topography. *1–2*: observation sites in Pre-Cenozoic bedrocks (*1*) and Late Cenozoic sediments (*2*); *3*: town. Numbers in circles refer to sub-basins: 1: Mondy; 2: Khoitogol; 3: Turan; 4: Tunka; 5: Tory; 6: Bystraya; letters in white squares refer to deformation zones: a: Kharadaban; b: Turan; c: Nilovsky; d: Badary sand ridge; e: Elovsky; f: Zurkuzun. **b**: fragment of the map of crustal fault-block

and verifying the second stage results was performed with help of the RES2DINV program for 2D inversion (Marescot et al., 2003; Panissod et al., 2001), which automatically produced a model of local resistivity using the data of VES profiles. The procedure of forward modeling was used for calculating an apparent resistivity, and the nonlinear optimization by the least-squares method was used for inversion modeling. When applying the optimization method, an effort was made to iteratively diminish the difference between calculated and measured values of the apparent resistivity until there is a good match between the model results and the geometry of the blocks. The value of the differences between observed and modeled values was expressed in terms of a mean-square error.

It is important to note that when constructing geoelectric models in the interpretation process of field electrical survey data, all available a priori data, including hydrogeological, were taken into account. Depending on the geological context and the region studied, the primary factors controlling the porosity and water saturation could be either the lithological, stratigraphical, hydrogeological or petrophysical parameters. Therefore, we applied Archie's law for evaluating resistivity values. As a result of the data interpretation, quantitative estimates of electrical parameters and thickness of sedimentary sections were obtained. The estimates, in turn, allowed us to identify complex tectonic structures, delineating permafrost areas, as well as refining the model of the deep basin architecture.

4. Near-surface tectonics of rift basins

The structural and tectonophysical investigations of the rift basins of the Baikal region show that their structure is controlled by fault tectonics, and the sedimentary cover is fractured (Lunina and Gladkov, 2004, 2007, 2008). Peculiarities of fault manifestations and associated tectonic deformations strongly depend on the degree of rocks consolidation and their granulometric composition (Gladkov and Lunina, 2004). Fractures, both with and without displacements, are the most widespread soft and shallow deformation features in the sediments. They developed everywhere but with different intensities. The greatest intensity is typical of fault zones where the fractures constitute dense networks such as in fractured and crushed zones (Fig. 2b). Fractures in a sedimentary layer containing a significant quantity of large debris are of special interest. In contrast to sandy and clay sediments, tectonic fractures can practically always be found and traced on split pebbles and boulders of hard rocks (Fig. 2a).

Traces of sliding and impact on pebbles and boulder surfaces (Fig. 2d) as well as clastic dikes (Fig. 2c) propagated locally along fault planes. Slickenslides and striated pebbles occur quite rarely in the Baikal region. Instead, sedimentary dikes are often associated with seismic shaking (Obermeier, 1996), and formed in close relation with active fractures at different depths.

Folds (Fig. 2e) and seismites (Fig. 2f) resulting from ground liquefaction during earthquakes are observed along active fault zones within a band whose width ranges from several hundred meters to a few tens kilometers. Similar structures are observed in different parts of the Baikal region (Gladkov and Lunina, 2010; Gladkov et al., 2005; Lunina and Gladkov, 2007). However, due to the East Siberian climatic and geotectonic conditions, it is possible to find both cryogenic and seismogenic deformations. We used field criteria listed in many publications (Obermeier, 1996; Sims, 1975, and others) to identify the seismogenic origin of such structures. With respect to the study area, the problem is especially discussed in Gladkov and Lunina, 2010.

We focused our study on these soft sediment deformation features, thus analyzing their localization relative to the main fault planes, damage fault zones and basement blocks. We addressed also a tectonophysical analysis of strike and dip of linear structures and attempted regional correlations of the inferred results with data for bedrocks and geomorphology in order to trace major faults over large distances.

5. Impact of near-surface tectonics on geoelectric parameters

A comparison between the results of surface mapping of basement-involving fault-blocks and geoelectric investigations was carried out with most detail for the Tunka, Barguzin and Muya basins located in the southwestern, central and northeastern parts of the Baikal rift zone, respectively (Fig. 1). Altogether, more than 30 profiles from 20 to 60 km in length were interpreted. As examples, several sections illustrating coincidence of faults with geoelectric boundaries or anomalies, as well as basement relief models reflecting peculiarities of deep basin structure, are represented and discussed below.

structure (full map is published in Lunina and Gladkov (2004)) and location of the geoelectric profiles discussed in text. *1*: basin filled by Cenozoic sediments; *2*: crystalline basement; *3*: geoelectric profile and its number; *4*: identified (a) and supposed (b) faults and their direction and dip angle; *5*: thermal springs; *6*: Quaternary volcanoes. **c**: 3D image of the basement surface in the central part of the basin from Nevedrova and Epov (2003). **d–e**: geoelectric sections on profiles 9 and 7; Fig. 3b for locations. *1*: heterogeneous part of the section, Quaternary sediments ($\rho = 180–450\ \Omega{\cdot}m$); *2*: presumptively rough-debris, Upper Miocene-Pliocene ($\rho = 85–180\ \Omega{\cdot}m$); *3*: conductive layer, Miocene ($\rho = 8–30\ \Omega{\cdot}m$); *4*: basement rocks ($\rho < 1000\ \Omega{\cdot}m$); 5: basement rocks ($\rho > 2000\ \Omega{\cdot}m$); black lines show faults crossing profiles from Fig. 3b.

Fig. 3. Bassin de rift de Tunka, Fig. 1 pour la localisation : **a** : topographie régionale. *1–2* sites d'observation dans le substratum pré-cénozoïque *(1)* et des sédiments du Cénozoïque supérieur *(2) ; 3 :* ville. Les chiffres entourés de cercles représentent des sous-bassins : 1 : Mondy ; 2 : Khoïtogol ; 3 : Turan ; 4 : Tunka ; 5 : Tory ; 6 : Bystraya ; les lettres dans les carrés blancs représentent les zones de déformation ; a : Kharadaban ; b : Turan ; c : Nilovsky ; d : chaîne sableuse de Badary ; e : Elovsky ; f : Zurkuzun. **b** : fragment de la carte de la structure crustale bloc-faille (la carte complète est publiée in Lunina et Gladkov (2004) et la localisation des profils géo-électriques est discutée dans le texte). *1 :* bassin rempli de sédiments cénozoïques ; *2 :* soubassement cristallin ; *3 :* profil géo-électrique et son numéro ; *4 :* failles identifiées (a) et supposées (b), avec leur direction et l'angle de pendage ; *5 :* sources thermales ; *6 :* volcans quaternaires. **c** : image 3-D de la surface du soubassement dans la partie centrale du bassin d'après Nevedrova et Epov (2003). **d–e** : sections géo-électriques dans les profils 9 et 7 ; Fig. 3b pour la localisation. *1 :* partie hétérogène de la section, sédiments quaternaires ($\rho = 180–450\ \Omega{\cdot}m$) ; *2 :* débris grossiers présumés Miocène supérieur-Pliocène ($\rho = 85–180\ \Omega{\cdot}m$) ; *3 :* lit conducteur, Miocène ($\rho = 8–30\ \Omega{\cdot}m$) ; *4 :* soubassement rocheux ($\rho < 1000\ \Omega{\cdot}m$) ; *5 :* soubassement rocheux ($\rho > 2000\ \Omega{\cdot}m$) ; les lignes noires représentent les failles traversant les profils, d'après la Fig. 3b.

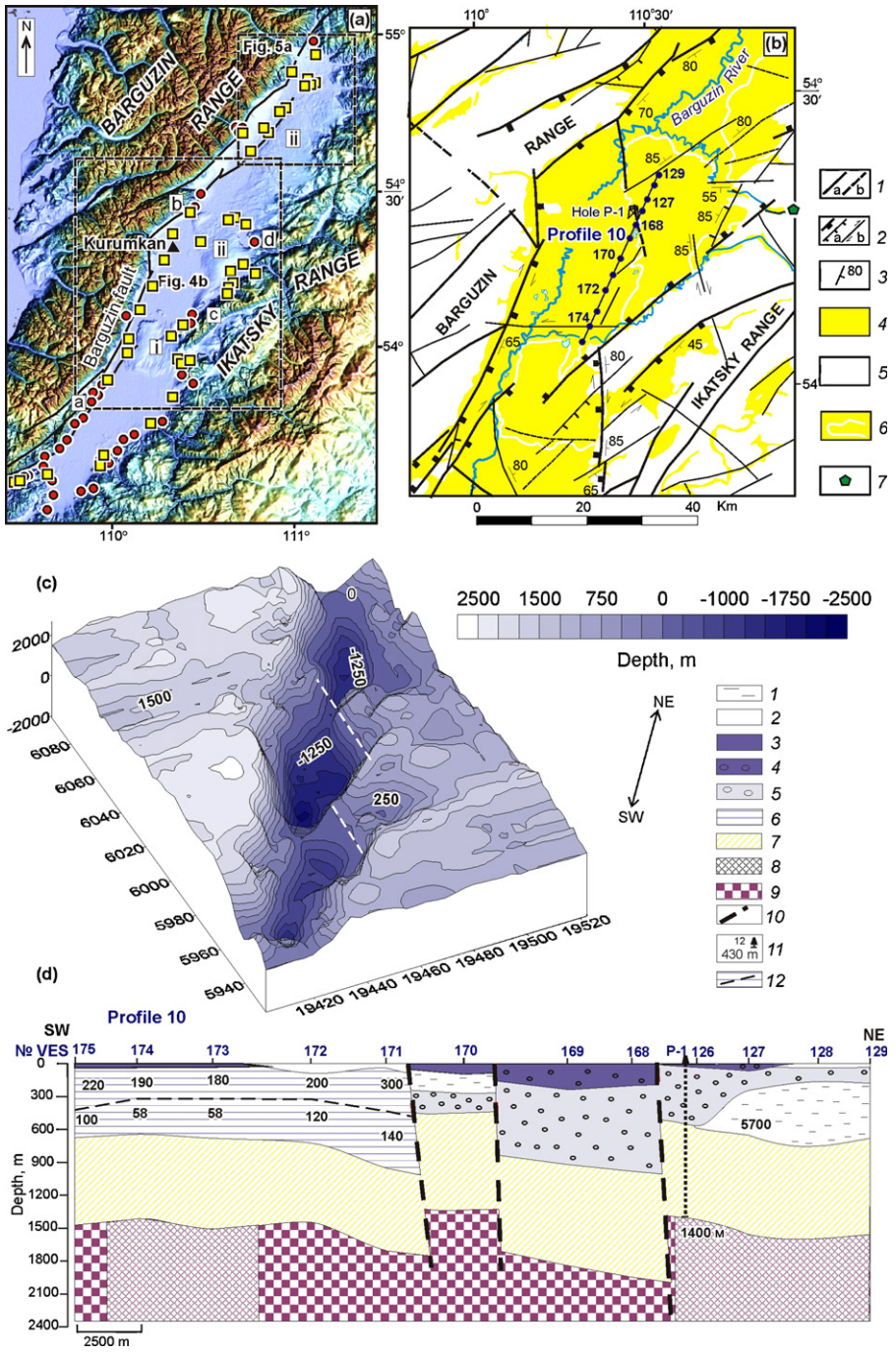

Fig. 4. The Barguzin rift basin; Fig. 1 for location. **a**: regional topography; see legends in Fig. 3a. Letters in white squares refer to spurs: a: Ulyun; b: Sakhulin; c: Argoda; d: Moleben; and to soft sediment deformation zones: i: lower sand ridge; ii: upper sand ridge. **b**: fragment of the map of crustal fault-block structure (full map is published in Lunina and Gladkov (2007)) and location of the geoelectric profile discussed in text. *1*: identified (a) and supposed (b) faults; *2*: normal faults (a) and strike-slip faults (b); *3*: direction and dip angle of fault; *4*: basin filled by Cenozoic sediments; *5*: crystalline basement; *6*: contours of sand ridges; *7*: thermal springs. **c**: 3D image of the basement surface from Epov et al. (2007). **d**: geoelectric section on profile 10; Fig. 4b for location. *1*: rocks with permafrost bands ($\rho = 2700–4500\ \Omega\cdot m$); *2*: permafrost ($\rho > 5000\ \Omega\cdot m$); *3*: Quaternary sediments ($\rho = 300–500\ \Omega\cdot m$); *4*: Quaternary sediments with gravel ($\rho = 1600–2600\ \Omega\cdot m$); *5*: Upper Pliocene sediments with pebble ($\rho = 500–1200\ \Omega\cdot m$); *6*: Upper Pliocene sediments ($\rho = 100–600\ \Omega\cdot m$); *7*: Middle Pliocene sandy-argillaceous and diatomite layers ($\rho = 10–32\ \Omega\cdot m$); *8*: basement rocks ($\rho > 1200\ \Omega\cdot m$); *9*: basement rocks ($\rho < 1000\ \Omega\cdot m$); *10*: supposed faults from geoelectric data; *11*: hole, its number and depth; *12*: geoelectric boundary.

Fig. 4. Bassin de rift de Barguzin ; Fig. 3b pour la localisation : **a** : topographie régionale ; voir légende sur la Fig. 3a. Les lettres dans des carrés blancs représentent les éperons : a : Ulyun ; b : Sakhulin ; c : Argoda ; d : Moleben ; et des zones de déformation dans des sédiments tendres : i : crête sableuse inférieure ; ii : crête sableuse supérieure. **b** : fragment de la carte de la structure bloc-faille de la croûte, (la carte complète est publiée in Lunina et Gladkov (2007) et la localisation des profils géo-électriques discutée dans le texte). *1 :* failles identifiées (a) et supposées (b) ; *2 :* failles normales (a) et de

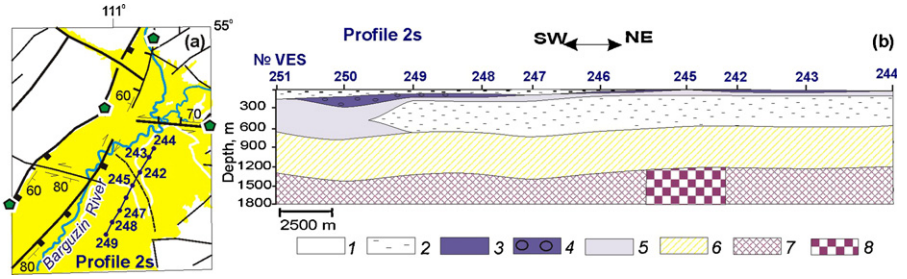

Fig. 5. Manifestation of NNW–SSE trending fault in ρ decreasing in a vertical zone, Barguzin rift basin: a: fragment of the map of crustal fault-block structure and location of the geoelectric profile 2s; legends in Fig. 4b; b: geoelectric section on profile 2s. *1*: rocks with permafrost bands (ρ = 1500–5000 Ω·m); *2*: permafrost ($\rho > 5000$ Ω·m); *3*: Quaternary sediments (ρ = 105–660 Ω·m); *4*: Quaternary sediments with gravel (ρ = 1020–1700 Ω·m); *5*: Upper Pliocene sediments (ρ = 125–400 Ω·m); *6*: Middle Pliocene sandy-argillaceous and diatomite layers (ρ = 72–200 Ω·m); *7*: basement rocks ($\rho > 3500$ Ω·m); *8*: basement rocks ($\rho < 1650$ Ω·m).

Fig. 5. Manifestation d'une faille de tendance NNW-SSE à ρ décroissant dans une zone verticale du bassin de rift de Barguzin : a : fragment de carte de la structure crustale bloc-faille et localisation du profil géo-électrique 2s ; légendes sur la Fig. 4b ; b : section géo-électrique dans le profil 2s *1 :* roches avec bandes de permafrost (ρ = 1500–5000 Ω·m) ; *2 :* permafrost ($\rho > 5000$ Ω·m) ; *3 :* sédiments quaternaires (ρ = 105–660 Ω·m) ; *4 :* sédiments quaternaires à graviers (ρ = 1020–1700 Ω·m) ; *5 :* sédiments du Pliocène supérieur (ρ = 125–400 Ω·m) ; *6 :* lits argilo-sableux et diatomitiques du Pliocène moyen (ρ = 72–200 Ω·m) ; *7 :* soubassement rocheux ($\rho > 3500$ Ω·m) ; *8 :* soubassement rocheux ($\rho < 1650$ Ω·m).

5.1. Tunka basin

In the central part of the Tunka Basin, where the geoelectric investigations were carried out, the example of the Kyngarga fault is especially representative (Fig. 3a, b). Before our research (Lunina and Gladkov, 2004), the fault was outlined only in the Tunka Range. It was scanned as an elongated contour of basement isolines in the 3D image (Fig. 3c), and on a series of geoelectric profiles (Fig. 3d, e). The Kyngarga fault is indicated by a zone of lower electric resistivity (ρ) values in basement rocks as compared with normal values, as well as a displacement of sedimentary layers, interpreted by a ρ difference. Other faults from the fault-block map are also shown on geoelectric sections (Fig. 3d, e). It is obvious that faults correlate well with changes in structure and dipping attitude of sedimentary strata and basement surface.

As a whole, the results of geoelectric research confirmed the "Baikal" asymmetry of the Tunka Basin: its largest subsidence is located along its northern side (Fig. 3c). However, the basin floor is complicated by a deformation zone in its central part. A NW-SE trending fault mapped by geological and structural data coincides with the eastern boundary of the shallow soft sediment deformation zone. The lowest basement surface is found at 3700 m and is located ca. 2 km from the Malyi Sagan-Nur Lake to the north.

5.2. Barguzin basin

The nearly north-south trending faults occupy a particular place in the Barguzin basin compared with the obvious domination of the NE-SW trending faults elsewhere (Fig. 4a). Most of these faults are aligned in a wide zone between 110°00′ and 110°30′ East long. (Fig. 2 in Lunina and Gladkov (2007)). When comparing the results of deep geoelectric investigations with the fault-block map (Fig. 4b), it was found that the nearly north-south trending fault in the central part of depression marks a boundary between the main basement sag and the subvertical upper sandy height (Fig. 4c). In the geoelectric section (Fig. 4d), the fault is expressed by ∼ 10 km thick fracture system displacing the layers vertically.

The deep geoelectric investigations confirm also the occurrence of a regional fault in the northern part of the Barguzin basin (Fig. 5a). Below 1200 m depth, the NNW-SSE trending fault is identified in the basement by anomalous ρ values decreasing in a vertical zone (Fig. 5b).

The "Baikal" asymmetry is also typical of the Barguzin Basin: the sediment thickness reaches a maximum of 2500 m along its northwestern side (Fig. 4c) that confirms earlier conclusions (Solonenko, 1981). According to geoelectric data, the sand ridges smoothly connect at depth to the Ikatsky Range. They are separated from the main part of the basin by a series of faults. As a whole, the sand ridges area corresponds to a sub-basin, in which sedimentary thickness is less than in the main sag near the Barguzin Range.

5.3. Muya basin

In the Muya basin (Fig. 6a), peculiarities of geoelectric structure and their correlation with faults traced through morphological and structural data can be observed on separated profiles. On profile I, the faults mapped on the surface fall near the VES points N° 69 and 68, and between

décrochement (b) ; *3 :* direction et angle de pendage de la faille ; *4 :* bassin rempli de sédiments cénozoïques ; *5 :* soubassement cristallin ; *6 :* contours des crêtes sableuses ; *7 :* sources thermales. **c** : image 3-D de la surface du soubassement d'après Epov et al. (2007). **d** : section géo-électrique dans le profil 10 ; Fig. 4b pour la localisation : *1 :* roches avec bandes de permafrost (ρ = 2700–4500 Ω·m) ; *2 :* permafrost ($\rho > 5000$ Ω·m) ; *3 :* sédiments quaternaires (ρ = 300–500 Ω·m) ; *4 :* sédiments quaternaires à graviers (ρ = 1600–2600 Ω·m) ; *5 :* sédiments du Pliocène supérieur à galets (ρ = 500–1200 Ω·m) ; *6 :* sédiments du Pliocène supérieur (ρ = 100–600 Ω·m) ; *7 :* lits argilo-sableux et diatomitiques du Pliocène moyen (ρ = 10–32 Ω·m) ; *8 :* soubassement rocheux ($\rho > 1200$ Ω·m) ; *9 :* soubassement rocheux ($\rho < 1000$ Ω·m) ; *10 :* failles supposées, d'après les données géo-électriques ; *11 :* creux, son numéro et sa profondeur ; *12 :* limite géo-électrique.

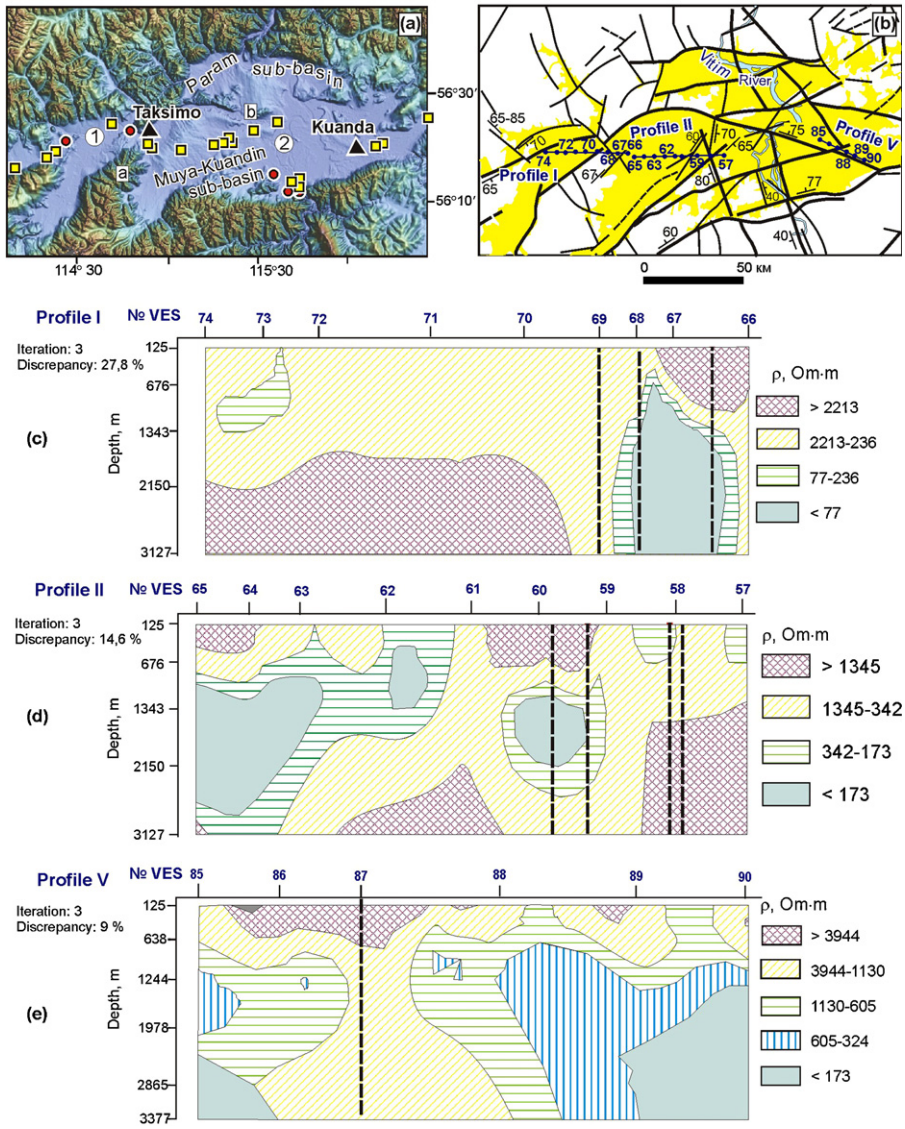

Fig. 6. The Muya rift basin; Fig. 1 for location. a: regional topography; legends in Fig. 3. **a**. Numbers in circles refer to basins: 1: Ulan-Makit; 2: Muya; letters in white squares refer to soft sediment deformation zones: a: Taksim; b: Param-Muya. **b**: fragment of the map of crustal fault-block structure (full map is published in Lunina and Gladkov (2008)) and location of the geoelectric profiles discussed in text; legends in Fig. 3b. **c–e**: geoelectric sections on profiles I, II and V, two-dimensional inversion; dotted lines show faults crossing profiles from Fig. 6b.

Fig. 6. Bassin de rift de Muya ; Fig. 1 pour la localisation. **a** : topographie régionale ; légendes en Fig. 3. *1 :* Ulan-Makit ; *2 :* Muya. Les lettres dans les carrés blancs représentent des zones de déformation dans des sédiments tendres. a : Taksim ; b : Param-Muya. b : fragment de la carte de la structure crustale bloc-faille (la carte complète est publiée in Lunina et Gladkov (2008)) et localisation des profils géo-électriques, discutée dans le texte ; légendes sur la Fig. 3b. **c–e** : sections géo-électriques dans les profils I, II et V, inversion bi-dimensionnelle ; les lignes en pointillés indiquent des failles traversant les profils (Fig. 6b).

points N° 66 and 67 (Fig. 6b, c). The faults are located rather close to each other. Essentially, they form a narrow fault network in the area of the Taksim soft sediment deformation zone, between the Ulan-Makit and Muya basins. Right after VES point N° 69, the geoelectric section is strongly changed at depths greater than 1000 m. Apart of the permafrost rock lenses, all vertical crustal sections crossing the fault zone located between VES points N° 69 and 66 are characterized by significantly lower ρ than the surrounding rocks.

Profile II runs from west to east entirely in the Muya basin (Fig. 6b, d). The sedimentary cover thickness reaches a maximum in 3500 to 4000 m at VES points N° 63 to 65, i.e., in its western part. At the VES point N° 69, the sedimentary thickness decreases to 2500 m. Two faults are traced between the VES points N° 59 and 60. East of the latter the basement depth reaches up to 800 m in agreement with the vicinity of the topographic shoulder of the Muya basin. It is worth to note that the basement ρ values decrease from 10,000 Ω·m to 1000 to 3000 Ω·m in the eastern part of the section, correlating with the fault zone in the area of the VES point N° 58.

Profile V is located in the southeastern part of the Muya basin (Fig. 6b, e). Except for the upper part of the section

where permafrost occurs, all crustal sections differ by their reduced rock resistivities. This is for instance the case in the southeastern part of the section where the profile is parallel to a large regional fault. At the VES point N° 87, this fault is intersected by another one. Right here, a tilt of the sedimentary layers occurs, and could be associated with an initial watercut near the fault. Instead, a thickness increase of high-resistance rocks most probably corresponds to permafrost. On the whole, one should notice the rather complex deep architecture of the Muya Basin that is due to the ubiquitous presence of permafrost layers with different thicknesses, and numerous faults complicating the overall geoelectric signatures. The maximum thickness of permafrost layers ranges form 5 to 25 m, increasing up to 50 to 400 m in river valleys. The thickness of the sedimentary cover varies also greatly, but is about 2000 m tick on the average. It decreases to a few several hundreds meters near the rift shoulders.

6. Discussion

Our research showed that the same faults mapped through combined geomorphological, tectonophysical, geological and structural data are detected by geoelectric methods in the basement and recorded also in the sedimentary cover at a shallower depth. Significant variations of electric parameters in a geological massif can be due to a redistribution of a conductive fluid. It is known that dehydrated rocks have a resistivity several times higher than in a natural environment; that is a presence of conductive fluids defines electric properties. The investigated basins correspond to areas where porosity and formation waters occur in sedimentary deposits. There are known mineral springs, including thermal ones, that are evidence of actively moving groundwaters. It appears that faults are path-ways for the fluids in such cases. If a fault is marked by a zone of reduced electrical resistivity one can suggest that most likely a heightened watercut is responsible of it. In other cases, faults are documented only by a displacement of layers with distinct geoelectric properties. This apparently characterizes locked faults where the lack of water increases frictional resistance.

Surface mapping, measurements of geoelectric sections and basement relief of the studied basins indicate the fault-block structure of both their sedimentary strata and basement. This conclusion agrees well with the regional morphology (Figs. 3a, 4a). Previous researchers noticed that uplifted deformation zones are typical of "Baikal" basins (Florensov, 1960; Sherman et al., 1973). Their number, forms and sizes can vary, but most often they are either isometric or elongated along the axis of a large depression. Sometimes the deformation zones branch off the rift shoulders of the basins and constitute local spurs, which connect to the basins margins. Such deformation features are rather typical for sedimentary basins developing during rifting (Konstantinovskaya et al., 2007). Analogue modeling shows that discrete basement faults significantly affect the localization, geometry and orientation of the shallower deformation zones (Byrne and Harris, 1992; Konstantinovskaya et al., 2007). In turn, contacts between basement blocks of different rheologies control the orientation and spacing of faults, and the localization of sub-basins in the overlying sand layers of the models (Higgins and Harris, 1997). Formation of the shallow deformation zones is more active under oblique extension (Mart and Dauteuil, 2000). In fact, heterogeneous distributions of crustal deformations under tectonic stresses, together with pre-existing basement faults, control their development and as a result individual blocks subside with different rates.

Asymmetry is another well-known peculiarity of the "baikal" basin structure. Mountain ranges bordering the Baikal sub-basins to the north and northwest are as a rule higher and steeper in comparison with those on the opposite side where mountains, though they have Alpine-type peaks, are rather low compared to the overall elevation of the basins.

The main characteristics of tectonic structures of the Tunka, Barguzin and Muya basins are similar to those of other large depressions of the Baikal region. One can conclude that the generalized tectonophysical model of the rift basin is defined first of all by the presence of shallow deformation zones, an asymmetric morphology, and the fault-block structure of the sedimentary layers and the subsurface part of the crystalline basement.

7. Conclusion

The integrated structural, tectonophysical and geoelectric investigations in the Baikal region allowed to demonstrate that the basin structure was controlled by fault tectonics, and that the sedimentary cover was broken by fractures rooted in the crystalline basement. The regional survey of deformational structures in the sedimentary deposits, together with the crushed and fractured zones at the edge of individual crystalline-basement rocks, allowed one to reveal hidden faults that can be both seismogenic and pathways for fluids expelled from the overburden during earthquakes. Additional geoelectric measurements can provide novel data on the faults geometry at depth, their vertical displacement and degree of watercut along the faults. The good agreement among results inferred from different approaches should give a strong base to construct in the future three-dimensional models of fault-block structure of the crystalline basement beneath these sedimentary basins.

Acknowledgements

We thank Damien Delvaux and two other anonymous reviewers for their comments, which contributed to improve our manuscript. Our research was partly supported by the Siberian branch of the Russian Academy of Science and the Russian Foundation for Basic Research (grants No 09-05-92421 – EINSTEIN Consortium, No 10-05-00072).

References

Byrne, D., Harris, L.B., 1992. Fault patterns during normal and oblique rifting and the influence of basement discontinuities: application to

models for the tectonic evolution of the Perth Basin, Western Australia. In: Rickard, M.J., et al. (Eds.), Basement Tectonics 9. Kluwer Academic Press, Netherlands, pp. 23–42.

Chunga, K., Livio, F., Michetti, A.M., Serva, L., 2007. Synsedimentary deformation of Pleistocene glaciolacustrine deposits in the Albese con Cassano Area (southern Alps, northern Italy), and possible implications for paleoseismicity. Sedimentary Geology 196, 59–80.

Delvaux, D., Moeys, R., Stapel, G., Petit, C., Levi, K., Miroshnichenko, A., Ruzhich, V., San'kov, V., 1997. Paleostress reconstruction and geodynamics of the Baikal region, Central Asia, part 2. Cenozoic rifting. Tectonophysics 282, 1–38.

Epov, M.I., Dashevsky, Yu.A., El'tsov, I.N., 1990. Automated system of interpretation of electro-magnetic sounding. SB RAS Press, Novosibirsk, 29 p. (in Russian).

Epov, M.I., Nevedrova, N.N., Sanchaa, A.M., 2007. A geoelectric model of the Barguzin basin in the Baikal rift zone. Russian Geology and Geophysics 48, 626–641.

Florensov, N.A., 1960. Mesozoic and Cenozoic basins of the Baikal area. AS USSR Press, Moscow-Leningrad, 258 p. (in Russian).

Gladkov, A.S., Lunina, O.V., 2004. Fractures in Late Cenozoic sediments: New possibilities for structural analysis. Doklady Earth Sciences 399, 1071–1073.

Gladkov, A.S., Lunina, O.V., 2010. Seismites of the southern East Siberia: research problems and perspectives. Geodynamics & Tectonophysics 1, 249–272.

Gladkov, A.S., Lunina, O.V., Dzuba, I.A., Orlova, L.A., 2005. New data on the age of deformations in non-lithified sediments of the Tunka rift depression. Doklady Earth Sciences 405, 1175–1178.

Higgins, R.I., Harris, L.B., 1997. The effect of cover composition on extensional faulting above reactivated basement faults: results from analogue modeling. Journal of Structural Geology 19, 89–98.

Hippolyte, J.-C., 2001. Palaeostress and neotectonic analysis of sheared conglomerates: Southwest Alps and southern Apennines. Journal of Structural Geology 23, 421–429.

V.K. Khmelevsky, V.A. Shevnina (Eds.). 1988. Electrical sounding of geological medium. Moscow State University Press, Moscow, part 1, 170 p., 1992, part 2, 200 p. (in Russian).

Konstantinovskaya, E.A., Harris, L.B., Poulin, J., Ivanov, G.M., 2007. Transfer zones and fault reactivation in inverted rift basins: Insights from physical modeling. Tectonophysics 441, 1–26.

Levi, K.G., Sherman, S.I., Plyusnina, L.V., Logotchev, N.A. (Eds.), 1982. Map of neotectonics of the Baikal and Trans-Baikal territories. Nauka, Institute of the Earth's Crust, Irkutsk (in Russian).

Levi, K.G., Miroshnichenko, A.I., San'kov, V.A., Babushkin, S.M., Larkin, G.V., Badardinov, A.A., Wong, H.K., Coleman, S., Delvaux, D., 1997. Active faults of the Baikal Basin. Bulletin Centre de Recherches Exploration Production Elf-Aquitaine 21, 99–434.

Logatchev, N.A., 2003. History and geodynamics of the Baikal rift. Russian Geology and Geophysics 44, 373–387.

Logatchev, N.A., Zorin, Y.A., 1987. Evidence and causes of the two-stage development of the Baikal rift. Tectonophysics 143, 225–234.

Lunina, O.V., Gladkov, A.S., 2004. Fault Structure of the Tunka Rift as a reflection of oblique extension. Doklady Earth Sciences 398, 928–930.

Lunina, O.V., Gladkov, A.S., 2007. Late Cenozoic fault pattern and stress fields in the Barguzin rift (Baikal region). Russian Geology and Geophysics 48, 598–609.

Lunina, O.V., Gladkov, A.S., 2008. Active faults and crustal stress in the northeastern flank of the Baikal rift system. Russian Geology and Geophysics 49, 113–123.

Marescot, L., Loke, M.H., Chapellier, D., Delaloye, R., Lambiel, C., Reynard, E., 2003. Assessing reliability of 2D resistivity imaging in mountain permafrost studies using the depth of investigation index method. Near Surface Geophysics 1 2, 57–67.

Mart, Y., Dauteuil, O., 2000. Analogue experiments of propagation of oblique rifts. Tectonophysics 316, 121–132.

Molnar, P., Tapponnier, P., 1975. Cenozoic tectonics of Asia: effects of continental collision. Science 189, 419–425.

Nevedrova, N.N., Epov, M.I., 2003. Deep geoelectric investigations in seismoactive areas. In: Geodynamics and geoecological problems of high-mountain regions, Painthouse Press, Moscow-Bishkek, pp. 153–163 (in Russian).

Obermeier, S.F., 1996. Use of liquefaction-induced features for paleoseismic analysis – An overview of how seismic liquefaction features can be distinguished from other features and how their regional distribution and properties of source sediment can be used to infer the location and strength of Holocene paleo-earthquakes. Engineering Geology 44, 1–76.

Panissod, C., Michot, D., Benderitter, Y., Tabagh, A., 2001. On the effectiveness of 2D electrical inversion results: an agricultural case study. Geophysical Prospecting 49, 570–576.

Papathanassiou, G., Pavlides, S., Christaras, B., Pitilakis, K., 2005. Liquefaction case histories and empirical relations of earthquake magnitude versus distance from the broader Aegean region. J. Geodynamics 40, 257–278.

Sherman, S.I., Medvedev, M.E., Ruzhich, V.V., Kiselev, A.I., Shmotov, A.P., 1973. Tectonics and volcanism of the Southwestern part of the Baikal rift zone. Nauka Press, Novosibirsk, 136 p. (in Russian).

Sims, J.D., 1975. Determining earthquake recurrence intervals from deformational structures in young lacustrine sediments. Tectonophysics 29, 141–152.

Solonenko, V.P. (Ed.), 1981. Seismogeology and detail seismic zoning of Pribaikal'e. Nauka Press, Novosibirsk, 168 p. (in Russian).

Tuttle, M.P., Dyer-Williams, K., Barstow, N.L., 2002. Paleoliquefaction study of the Clarendon-Linden fault system, western New York State. Tectonophysics 353, 263–286.